ORIGINAL ARTICLE

Mechanism of deflagration-to-detonation transitions above repeated obstacles

T. Obara · T. Kobayashi · S. Ohyagi

Abstract Experiments are carried out to investigate the mechanism of the deflagration-to-detonation transition (DDT). Because, this mechanism has relevance to safety issues in industries, where combustible premixed gases are in general use. A stoichiometric gas of oxygen and hydrogen (oxy-hydrogen) is ignited in a tube, repeated obstacles are installed, and the DDT behaviours are visualized using a high-speed video camera. The pitch and height of the repeated obstacles and the initial pressure of the oxy-hydrogen premixed gas are varied in an attempt to obtain the optimum conditions that cause DDT a short distance from the ignition source. The experiments identified DDT as being essentially caused by one of the following mechanisms: (1) A deflagration wave is accelerated in terms of a vortex, which is generated behind the obstacle, and the flame acceleration induces a secondary shock wave. Eventually, the shock–flame interaction ahead of the obstacle causes DDT via a very strong local explosion. (2) Each shock wave generated by relatively weak local explosions between the obstacles is not sufficient to cause DDT directly, but DDT results from an accumulation of shock waves. The detonation induction distance is also examined, taking into account the physical and chemical parameters of the obstacles and the oxy-hydrogen premixed gas.

T. Obara (✉) · T. Kobayashi · S. Ohyagi
Graduate School of Science and Engineering, Saitama University, 255 Shimo-Ohkubo, Sakura-ku, Saitama-shi, Saitama 338-8570, Japan
e-mail: tobara@mech.saitama-u.ac.jp

S. Ohyagi
e-mail: ooyagi@mech.saitama-u.ac.jp

1 Introduction

It is generally known that combustion waves propagated in a premixed gas can be classified as either deflagration waves or detonation waves. A detonation wave is not generated simultaneously with ignition, unless an extremely high ignition-energy is supplied to the premixed gas, but is produced via a deflagration-to-detonation transition phenomenon called DDT [1]. In a confined tube, DDT occurs without any difficulty if the premixed gas possesses a high reaction rate, or if the premixed gas is ignited in a small-diameter tube, or if the inner wall of the tube can be made rough, e.g., by equipping the tube with a spiral-coil. The technique of inserting a spiral-coil into a tube is commonly used to produce detonation waves. The role of the spiral-coil is to produce turbulent flow ahead of the deflagration wave, thus increasing the propagation velocity of the deflagration wave, causing DDT via a local explosion [1]. However, the ultimate phenomenon in DDT is somewhat uncertain, because the phenomenon occurs in a localized region during an extremely short period of time.

It has been argued that an obstacle influences flame acceleration by causing positive coupling between the flame and a turbulence [2]. An induction time gradient obtained by turbulent mixing leading to the initiation of a detonation wave is proposed as the SWACER mechanism [3]. An experimental study of DDT in a smooth tube filled with an oxy-hydrogen mixture showed that the turbulent motion of the flame triggered DDT, and the scale of the turbulence was also evaluated [4]. A deflagration wave, propagated at about half the Chapman–Jouguet (C–J) detonation velocity, has been

shown to cause successful detonation initiation [5]. A laser system has been used as a light source to visualize the onset of DDT and describe the various possible transition modes [1]. A photographic study of quasi-detonation waves in a rough tube was carried out to demonstrate the dual role of obstacles, such as the positive role of re-initiation, by providing a reflection surface for the shock wave, and the negative role of detonation attenuation [6,7]. The effects on flame acceleration of a re-circulation zone between orifice plates have been pointed out [8–11], and DDT under elevated temperature and pressure has also described [12]. Numerical simulations have also been performed, revealing that DDT depends strongly on obstacle spacing, and suggesting two important effects: formation of perturbations increasing the flame surface area and formation of a Mach-stem between the obstacles [13]. Furthermore, for quasi-detonations, both the initial DDT and the succeeding detonation re-ignitions, occur when the Mach-stem created by the reflection of the leading shock wave from the bottom wall collides with an obstacle [14]. Experimental investigations of the effects of scale on detonation onset have shown that the detonation cell-width λ is a reliable scaling parameter for characterization of detonation onset conditions [15]. The transition mechanism from deflagration to a detonation wave has been explored by changing the configurations of the tube [6,16–18]. Changes in DDT behaviour with variations in the regularity of the cellular structure on the detonation front were also examined [19]. Experimental studies of reduction of the detonation transition distance showed that the distance was dependent on a reduced activation energy and a normalized heat of reaction [20]. DDT phenomena in a narrow channel were also investigated to determine an empirical equation for the detonation induction distance from an ignition source [21]. Although a great deal of effort has been devoted to studying DDT mechanisms by changing the experimental conditions, the final stage of DDT is still open to discussion. In particular, not much is known concerning the onset mechanism of a local explosion. Furthermore, the optimum spiral-coil dimensions for producing DDT a short distance from the ignition source have not yet been completely quantified. Therefore, much more research is obviously needed to understand the optimum conditions for causing DDT. Investigations concerning DDT behaviour and the detonation induction distance are of particular importance, not only with respect to countermeasures to detonation hazards, but also with respect to practical applications in pulsed detonation engines [20].

The present study addresses issues concerning DDT mechanisms above repeated obstacles, and experiments are carried out primarily by visualizing DDT phenomena. A stoichiometric premixed oxy-hydrogen gas is ignited in a tube equipped with repeated obstacles, and the DDT behaviours are visualized using a high-speed video camera. The pitch, d, and height, h, of the repeated obstacles, and the initial pressure of the oxy-hydrogen premixed gas, p_0, are varied to examine DDT mechanisms and to obtain the optimum conditions for causing DDT.

2 Experimental setup

Figure 1 shows a schematic diagram of the experimental setup. The detonation tube used in this experiment is constructed from a combustion tube of length 1.58 m and a dump tube of length 3.17 m, and has an inner cross-section of width 100 mm and height 100 mm. A plate of thickness 15 mm is installed on the bottom wall of the combustion tube, and thus the inner cross-section of the channel becomes 85 mm high by 100 mm wide. The combustion tube is filled with an oxy-hydrogen premixed gas; the dump tube is evacuated in advance. The two tubes are separated by inserting a mylar film of thickness 25 μm. The combustion channel has a volume of 1.3×10^{-2} m^3. A pair of optical-quality glass windows (BK7) of width 200 mm, height 100 mm, and thickness 25 mm is installed in the combustion tube for observation of DDT behaviours. A thin rubber plate is inserted in the space between the repeated obstacles and the glass window to ensure that the flow cannot pass through the side wall. A sparking plug is installed at the end-wall of the combustion tube, thus combustion waves propagate to the right. Also shown in Fig. 1 is a conventional double-mirror Z-configuration schlieren optical system for visualizing the density gradient through the combustion wave. A metal-halide light (LS-M350, 350 W, Sumita Optical Glass, Inc.) with an optical fibre is used as the light source in the schlieren system. A high-speed video camera (Ultra Cam HS-106E, nac Image Technology, Inc.) is used to visualize DDT behaviour, with an interframe time of 2 μs and an exposure time of 100 ns for each frame. This video camera can capture high-speed sequences of a total of 120 frames with resolutions of 410×360 pixels and with a wavelength range of 300–750 nm.

Another high-speed video camera (Phantom V7.3, Vision Research, Inc.) is used to observe the whole sequence of DDT behaviour with an interframe time of 17 μs and an exposure time of 1 μs for each frame. This video camera acquires monochromatic photographs of approximately 7×10^4 frames with a resolution of 272×120 pixels. Insertion of an iris near a knife edge facilitates visualization of the detonation phenomena; light emissions from DDT onset, in particular, are intense.

Figure 2 illustrates the configuration of the combustion tube in detail. Repeated obstacles are set up on the bottom wall of the combustion tube. Measuring stations are also mounted on the top wall; the distance of each measuring station from the sparking plug is shown in Table 1. Piezoelectric-

Fig. 1 Schematic diagram of the experimental setup; the premixed gas is ignited at the left end-wall of the combustion tube; the DDT phenomenon is visualized, using a high-speed video camera, by the conventional double-mirror Z-configuration schlieren optical method
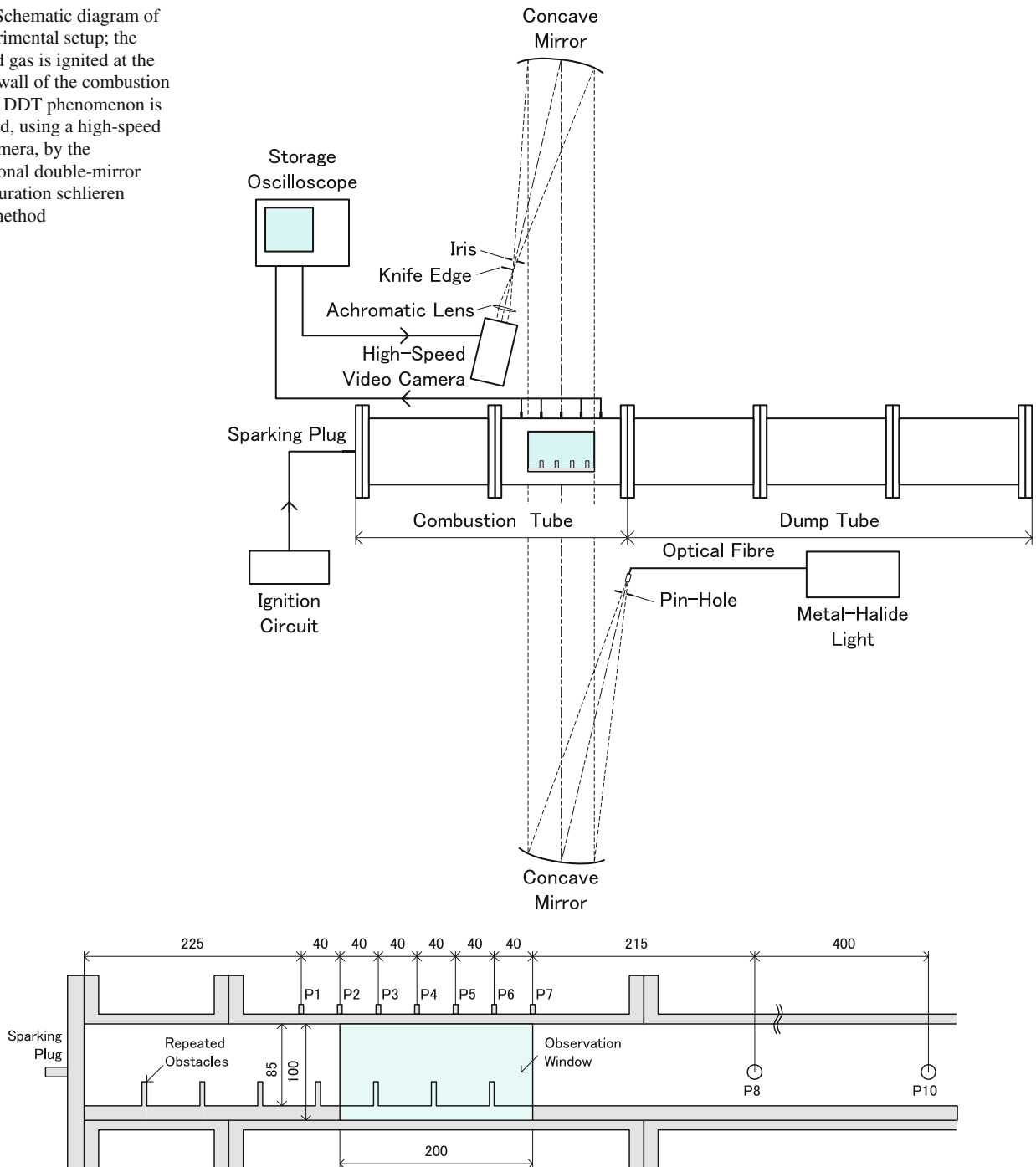

Fig. 2 Schematic diagram of the combustion tube; the repeated obstacles are installed on the bottom wall of the tube; measuring stations named P1 to P7 are installed on the top wall, P8 and P10 are installed on the side wall; the phenomena occurring in an area of width 200 mm and height 85 mm are visualized

type pressure transducers (113A24, response time: less than 1 μs, PCB Piezotronics, Inc.) are installed at measuring stations P1 to P10, and the pressure signals are recorded with a storage oscilloscope (ScopeCorder DL-750, 10 MS s^{-1}, Yokogawa Electric Corp.). The video camera is triggered by the output signal from the pressure transducer mounted at measuring station P1.

Figure 3 illustrates the configuration of the repeated obstacles, and Table 2 shows their dimensions. The channel height, H, and the obstacle width, w, are constant at 85 and 5 mm, respectively. However, the obstacle pitch, d, is varied as 20, 40, and 60 mm, and the height, h, is varied as 15 and 25 mm. Thus, obstacles of seven kinds are examined, including the case with no obstacle inserted ($h = 0$). The total volume of

Table 1 Distance of each measuring station from the sparking plug

Measuring station	Distance from sparking plug (mm)
P1	225
P2	265
P3	305
P4	345
P5	385
P6	425
P7	465
P8	680
P10	1,080
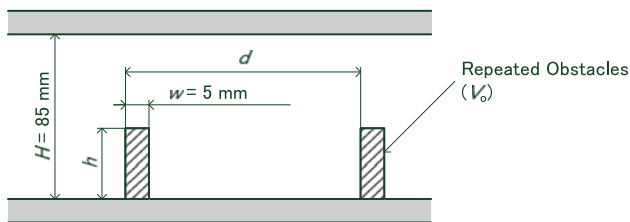
Fig. 3 Schematic diagram of the repeated obstacles; the pitch, d, and the height, h, are varied

Table 2 Configuration of the repeated obstacles

Parameter	Dimension
Channel height, H (mm)	85
Width, w (mm)	5
Pitch, d (mm)	20, 40, 60
Height, h (mm)	0 (without obstacle), 15, 25

Table 3 Experimental conditions of the test gas

Parameter	Conditions
Fuel	H_2
Oxidizer	O_2
Equivalence ratio, ϕ	1.0
Initial pressure, p_0 (kPa)	30, 50, 70
Initial temperature, T_0 (K)	298 ± 5

the obstacles is designated as V_o; this is calculated by multiplying the volume of each obstacle by the total number of obstacles in the combustion tube. Abbreviations are used to designate the obstacles, e.g., the obstacle of pitch $d = 60$ mm and height $h = 25$ mm is abbreviated to d60h25.

The experimental conditions of the test gas are shown in Table 3. The test gas used to fill the combustion tube is a stoichiometric premixed oxy-hydrogen gas, and the initial pressure, p_0, is varied as 30, 50, and 70 kPa. The test gas is premixed using a mixing tank of volume 2.3×10^{-2} m^3, and is stored for at least 12 h before being used. Every experiment is conducted at a room temperature of $T_0 = 298 \pm 5$ K.

3 Results

Under the given experimental conditions, the behaviours occurring in the combustion tube could be classified into the following three types.

1. A deflagration wave is propagated without causing DDT in the observation section.
2. DDT occurs as a result of interactions of the deflagration wave with shock waves generated by a relatively strong local explosion between the obstacles.
3. DDT occurs by an accumulation of the shock waves generated by the relatively weak local explosions between the obstacles.

This section deals with these three typical phenomena by showing high-speed schlieren photographs along with pressure histories and soot-track records.

3.1 Propagation of deflagration wave without causing DDT

As an example, sequential schlieren photographs of propagation of a deflagration wave are shown in Fig. 4; these were obtained in the absence of repeated obstacles. These photographs were taken with an interframe time of 17 µs, but show extracts of typical behaviours. The time shown in each frame indicates the elapsed time from ignition, and the mounted position of the pressure transducer is labelled as P4. The first frame, at $t = 1.544$ ms, shows that a deflagration wave propagates to the right. The deflagration wave could essentially be propagated by the mechanisms of heat conduction and molecular diffusion through the flame front, thus the chemical reaction rate is not so fast that no strong light emission from the flame is observed. As the flame propagates, it is seen that the flame front has a round shape, accompanied by a number of wrinkles on the surface, although wrinkles caused by thermo-diffusive effects lie outside the scope of this paper. Since the flame propagated in the depth direction is attached to the optical windows, the wrinkles disappear at the rear of the flame. The average flame-propagation velocity from the first frame to the second frame is estimated to be approximately 373 m s^{-1}, which is below the speed of sound (540 m s^{-1}), 380 m s^{-1} from the second frame to the third frame, reaching the local maximum velocity, and then decreasing to approximately 310 m s^{-1} from the fifth frame to the sixth frame. As the flame propagates, the end-wall effects do not act on the flame, resulting in flame deceleration.

Figure 5 shows the pressure histories and output signals from ionization probes; these are simultaneously recorded with the schlieren photographs, as shown in Fig. 4. The mounted positions of the pressure transducers and the ionization probes are designated in each history. The vertical axis indicates the non-dimensional pressure, p/p_0, and the
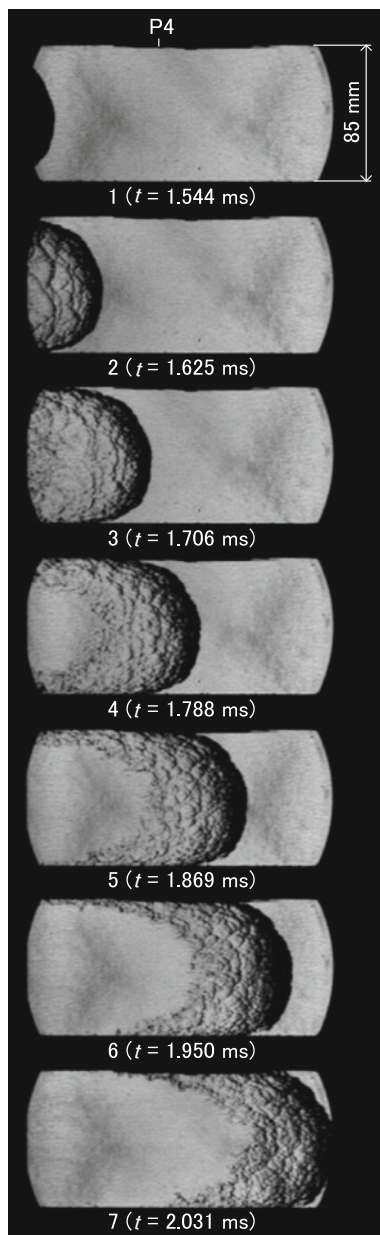
Fig. 4 Schlieren photographs showing propagation of the deflagration wave in the absence of repeated obstacles; t elapsed time from ignition; exposure time: 1 μs; test gas: $2H_2 + O_2$, $p_0 = 50$ kPa

Fig. 5 Pressure histories corresponding to Fig. 4; t elapsed time from ignition; without obstacles; test gas: $2H_2 + O_2$, $p_0 = 50$ kPa

velocity of approximately 2.77 km s^{-1}. The retonation wave is reflected for a second time at the end-wall. The pressure history of P10 decreases to a negative value behind the detonation wave because of the thermal effects on the pressure transducer. In the absence of repeated obstacles, DDT does not occur at the observation section and only the deflagration wave is propagated, but DDT occurs far from the sparking plug, because these experimental conditions satisfy the criteria for the existence of detonation [22].

3.2 DDT caused by shock–flame interactions between obstacles

As an example of DDT occurring between repeated obstacles, Fig. 6 shows sequential schlieren photographs with an interframe time of 6 μs and an exposure time of 100 ns. The obstacle d60h25 is inserted on the bottom wall of the combustion tube. The initial pressure of the test gas is $p_0 = 50$ kPa. The mounted positions of the pressure transducers are labelled as P3 and P5, respectively. In the first frame, $t = 1.409$ ms, a deflagration wave, F, has just approached the obstacle on the left-hand side, preceded by a weak shock wave, S. The deflagration wave has a round shape, as previously shown in Fig. 4, so the curved shock wave is reflected from the top wall, and thus complicated shock-reflection patterns are revealed ahead of the deflagration front. The precursor shock wave is also reflected from the left obstacle, thus the interaction between the reflected shock wave and the flame has already been initiated in the first frame. This interaction makes the flame decelerate; the reason is discussed below. A series of vortices, V, are also produced from the corner of the

horizontal axis indicates the elapsed time from ignition, t. The pressure increases, corresponding to the propagation of weak shock waves, caused by the acceleration of combustion waves, but the values of the pressure increases are small. The pressure suddenly increases near measuring station P10, which is downstream of the observation window, and an output signal from the ionization probe is detected simultaneously. This pressure increase shows that the deflagration wave is transited to a detonation wave between measuring stations P8 and P10, thus a shock wave, called a retonation wave, is propagated in the upstream direction with a
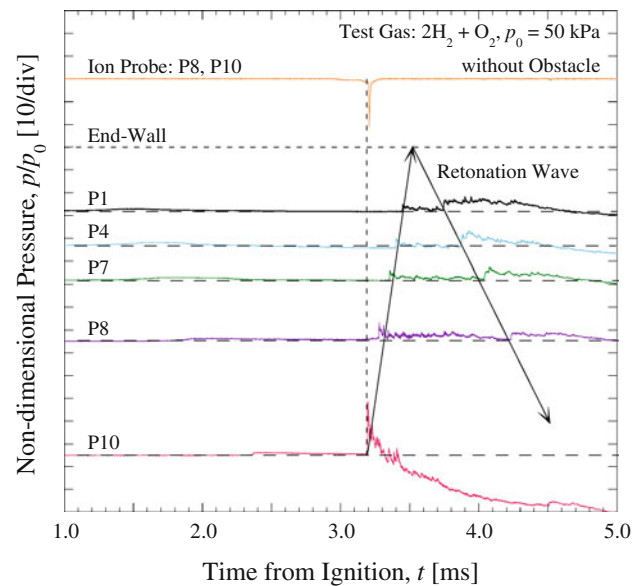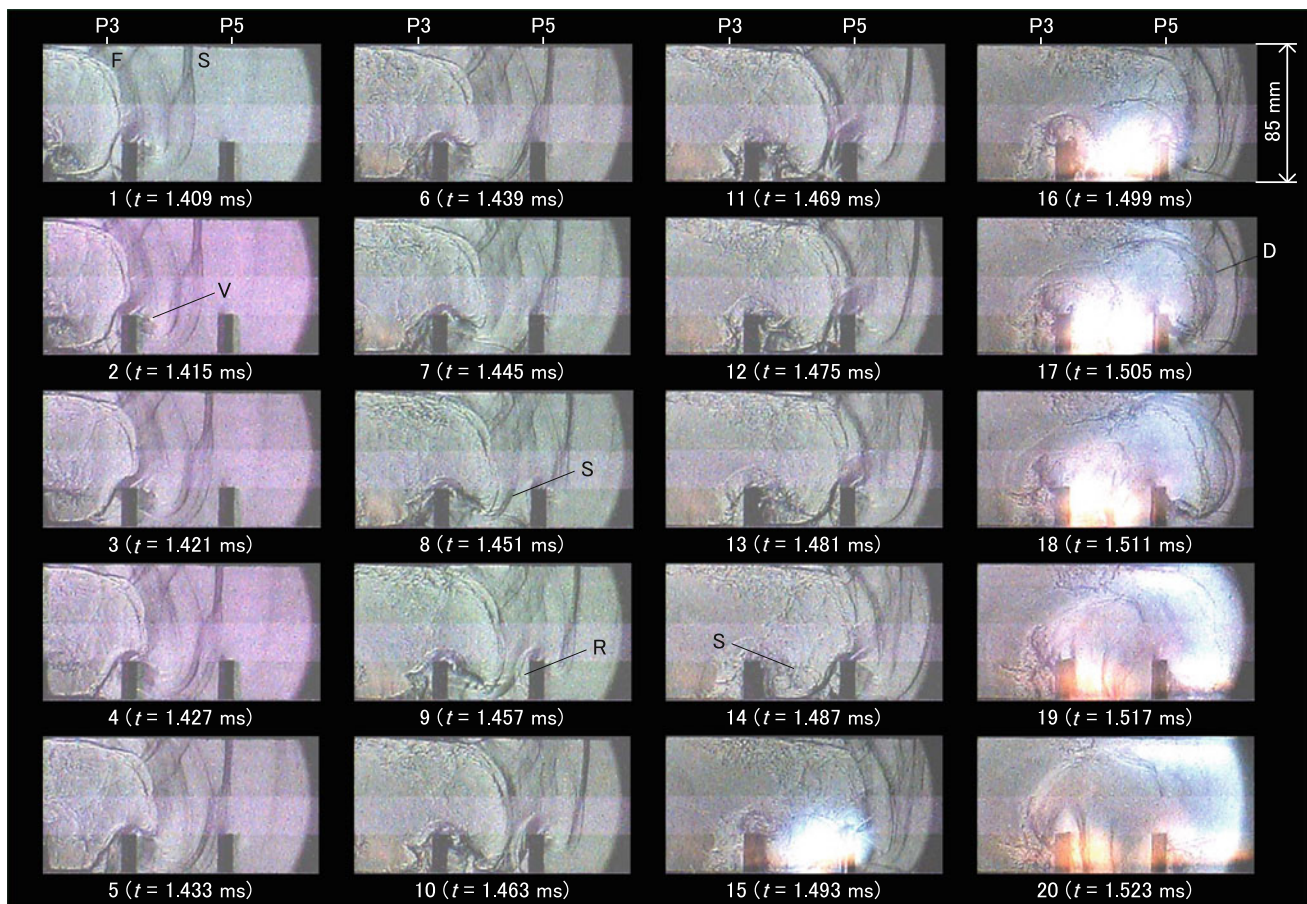
Fig. 6 Schlieren photographs showing DDT processes occurring between the obstacles; t elapsed time from ignition; exposure time: 100 ns; obstacle: d60h25; test gas: $2H_2 + O_2$, $p_0 = 50$ kPa; D detonation wave; F deflagration wave; R reflected shock wave; S shock wave; V vortex

left obstacle, because the precursor shock wave is diffracted from the obstacles by interaction with expansion waves generated from the obstacle corners. The expansion waves also make the lower part of the shock wave thicker, and the diffracted shock wave is reflected from the bottom wall between the obstacles. Mach-stem formation on the reflected shock wave is not observed near the bottom wall since complicated flow fields are produced in this region. When the deflagration wave, F, encounters these vortices regions from the fifth frame, $t = 1.433$ ms, the vortices cause the deflagration wave to accelerate, as if the deflagration wave is almost engulfing the vortices. Because the clockwise flow is produced by the vortices, a part of the deflagration wave is accelerated by the flow-field in the vortices region. The obstacles do, therefore, fulfill a first role as a vortex generator, and each vortex plays a significant role in accelerating the deflagration wave to a higher propagation velocity. This acceleration of the deflagration wave induces a secondary shock wave, S, between the obstacles. Propagation of the secondary shock wave results in amplifications of succeeding vortices behind the obstacles. The incident shock wave is reflected from the bottom wall,

as shown in the fifth frame, $t = 1.433$ ms, and is propagated upward. Thus, mutual interactions occur between the reflected shock wave and the secondary shock wave. A part of the secondary shock wave is also reflected from the right obstacle, R, thus other shock–flame interactions are caused between the obstacles. The interaction of the reflected shock wave with the deflagration wave causes the deflagration wave to decelerate, because the flow toward the right obstacle is terminated by the reflected shock wave. Therefore, the deflagration wave, once accelerated by the vortex, is conversely decelerated by the reflected shock wave, and these effects generate unreacted gas pockets in front of the right obstacle. Since deflagration wave propagation is almost stopped, heat conduction from the deflagration wave to the unreacted gas pockets might occur for a relatively long period of time, so this behaviour might result in temperature enhancement of the unreacted gas pockets. The obstacles play a major role in vortex generation, and, as a secondary effect, unreacted high-temperature gas pockets are produced between the obstacles.

In the eleventh frame, $t = 1.469$ ms, the curved deflagration front propagated downward is just in contact with

the bottom wall, producing a wedge-like unreacted region near the bottom wall. In this wedge-like unreacted region, the reflected shock waves interact mutually; one reflection is from the bottom wall, and the other is from the right obstacle, as previously mentioned. A local explosion shock wave, revealed by a semi-circular shape, S, is generated in the fourteenth frame, $t = 1.487$ ms, and propagated upward, even though light emission has not been observed behind the shock wave at this stage. In the fifteenth frame, $t = 1.493$ ms, a large amount of white light is emitted from the concave region, and this clearly indicates the occurrence of a strong local explosion. The centre of the local explosion coincides with the deflagration front near the bottom wall, thus the local explosion might originate from a shock–flame interaction mechanism [23]. There is so little unreacted gas close to the bottom wall that the predominant light emission occurs just after the local explosion shock wave interacts with the previously mentioned unreacted gas pockets.

In the seventeenth frame, $t = 1.505$ ms, the deflagration wave is transited to a detonation wave, D, or rather a detonation wave is produced by this local explosion. However, there is insufficient information in this schlieren photograph to determine if any of this is the detonation wave. Thus, the onset of the detonation wave will be ascertained later, along with observation of the pressure histories and soot-track records. In addition, light emission between the obstacles continues for a relatively long period of time. In particular, it is noteworthy that the colour of the light changes from white to orange with time. The white light at the time of the local explosion onset might be the chemiluminescence principally emitted by OH radicals, which have a
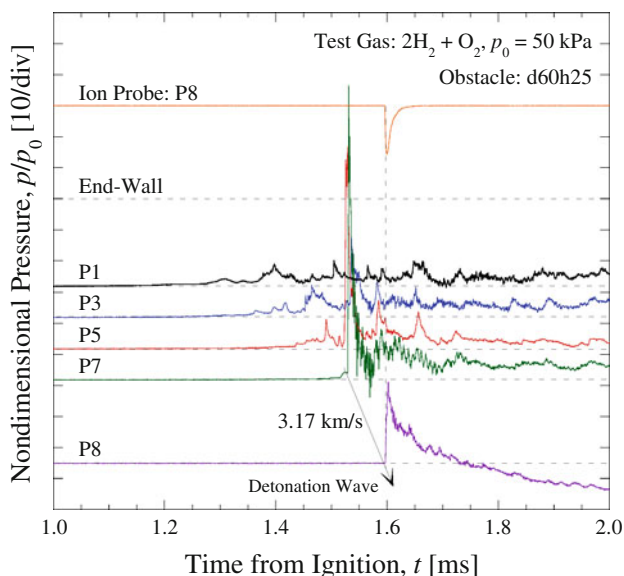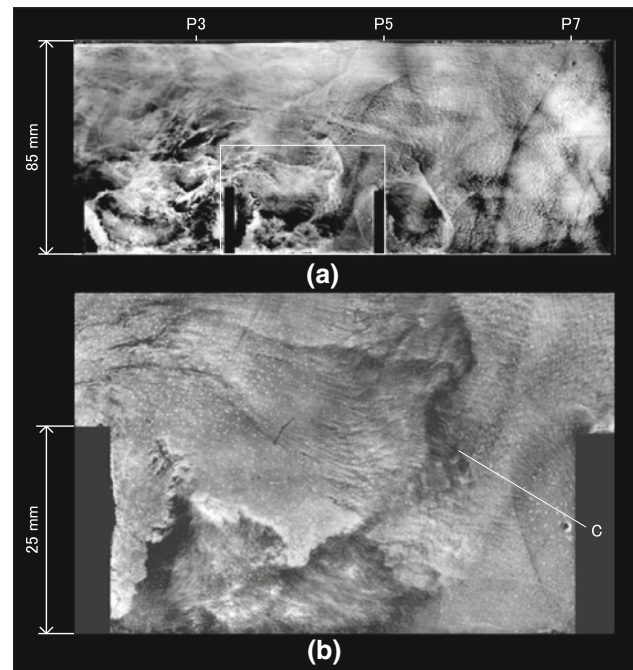

Fig. 8 Soot-track record corresponding to Fig. 6; obstacle: d60h25; test gas: $2H_2 + O_2$, $p_0 = 50$ kPa; C origin of cellular pattern

wavelength range of approximately 300 nm, and the eventual change to orange could signify emission from H_2O, which has a longer wavelength range.

Figure 7 shows pressure histories simultaneously acquired with schlieren photographs, as shown in Fig. 6. A small pressure rise at P1 corresponds to the precursor shock wave, generated by acceleration of the deflagration wave. The pressure histories measured at P5 and P7 show that the maximum pressure exceeds the initial pressure by factors of approximately 66 and 96, respectively. These intense pressure increases provide evidence that the detonation wave is established between measuring stations P5 and P7, as previously shown in Fig. 6. The pressure at P5 records the impulsive pressure twice; the secondary pressure rise corresponds to propagation of the detonation wave, as shown in the eighteenth frame of Fig. 6. The propagation velocity of the detonation wave from P7 to P8 is estimated to be approximately 3.17 km s^{-1}, and this value exceeds the C–J detonation velocity of approximately 2.80 km s^{-1}. Therefore, an overdriven detonation wave is propagated at the onset of DDT, as is generally accepted.

Figure 8a shows a soot-track record of the observation section, and Fig. 8b shows a magnification of the rectangular section in Fig. 8a. Since the soot-track record is obtained by covering an optical window with a soot-coated aluminum plate, the soot-track record cannot be obtained simultaneously with the schlieren photographs. The soot-track record is, therefore, obtained under the same experimental conditions as those in Fig. 6. These figures indicate that the cellular
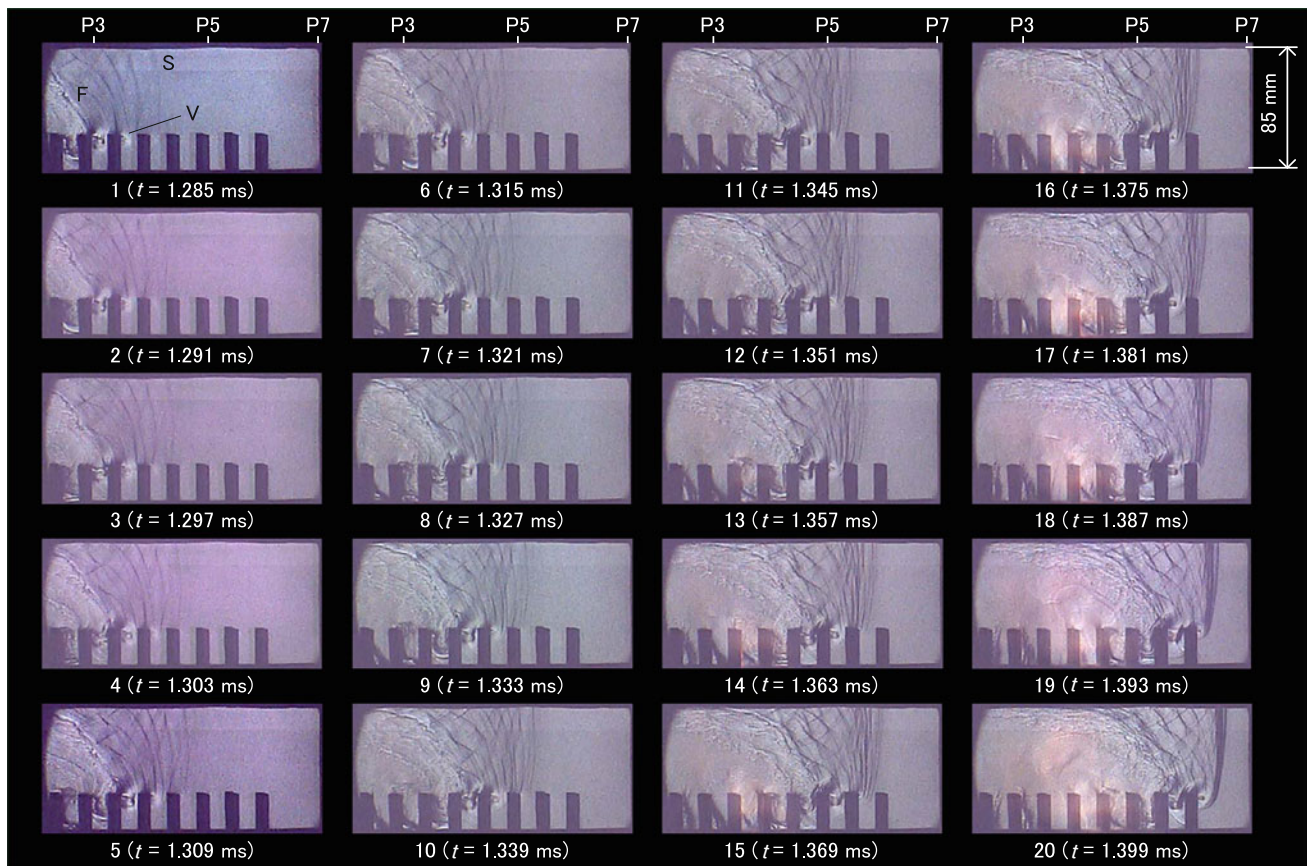

Fig. 7 Pressure histories corresponding to Fig. 6; t elapsed time from ignition; obstacle: d60h25; test gas: $2H_2 + O_2$, $p_0 = 50$ kPa

Fig. 9 Schlieren photographs showing DDT process occurring by accumulation of weak shock waves; t elapsed time from ignition; exposure time: 200 ns; obstacle: d20h25; test gas: $2H_2 + O_2$, $p_0 = 50$ kPa; F deflagration wave; S shock wave; V vortex

patterns originate in front of the obstacle, C, and this position is close to that of the local explosion onset, as shown in Fig. 6. Therefore, the shock wave generated by acceleration of the deflagration wave is reflected from the obstacle and interacts with the deflagration wave, so it induces a local explosion to trigger the detonation wave. The cellular patterns disappear behind the obstacle, because expansion waves originating at a corner of the obstacle result in a reduction in the temperature and pressure. Thus, the preceding shock wave is separated from the reaction front, causing temporary quenching of the detonation wave. However, the cellular patterns are re-initiated from the bottom wall, because the detonation wave is re-initiated by the reflected shock wave from the bottom wall [24–26].

3.3 DDT caused by accumulation of weak shock waves

Figure 9 shows sequential schlieren photographs, with an interframe time of 6 μs and an exposure time of 200 ns, of another type of DDT process. The d20h25 obstacle is inserted, and the initial pressure of the test gas is $p_0 = 50$ kPa. The obstacle pitch is, therefore, the only condition which is different from the conditions in Fig. 6. As with the behaviours

in Fig. 6, multiple precursor shock waves, S, and a deflagration wave, F, propagate to the right. Vortices, V, emerge sequentially between the obstacles. Since the pitch of the obstacle is less than that in Fig. 6, smaller vortices might be produced between the obstacles. Therefore, the acceleration of the deflagration wave by the vortices is not sufficient to cause a strong local explosion like that shown in Fig. 6. In other words, the volume of premixed gas in the concave region and the scale of the vortex are small, so the deflagration wave could not be accelerated sufficiently to induce an intense local explosion. Although sequential light emissions are also observed from the fourteenth to the twentieth frames, $t = 1.363–1.399$ ms, the colour of the light is observed to be orange and this behaviour is completely different from Fig. 6. This also provides evidence that the local explosion between the obstacles is not intense, and that relatively weak shock waves are induced and reflected from each concave region. As observed above, the flow-field behind the precursor shock wave becomes quite complicated, displaying mesh-like patterns, and producing a high-pressure and high-temperature region. The separation distance between the precursor shock wave and the deflagration front is gradually shortening. Also, the reflected shock waves from the top wall interact with the

reaction zone of the deflagration front, resulting in generation of more turbulent flame structures. The propagation velocity of the shock wave behind the precursor wave is higher, and this causes concentration of the weak shock waves. In the twentieth frame, $t = 1.363$ ms, the shock waves are overlapped, inducing a relatively strong shock wave, which is revealed as a thicker density gradient. Under these experimental conditions, however, DDT behaviour is not caused by shock wave concentration, but occurs at a downstream region of the observation section, as will be ascertained by investigating pressure histories.

Figure 10 shows pressure histories simultaneously recorded with the schlieren photographs, as shown in Fig. 6. In the pressure histories recorded at measuring stations P1 to P7, an impulsive pressure rise corresponding to DDT is not recorded, and the behaviours are qualitatively consistent with the observations of the schlieren photographs. In contrast, intense pressure rises are recorded at P8, and the time of the pressure increase coincides with output detection from the ionization probe. This provides evidence that DDT occurs between P7 and P8, and the detonation wave is propagated at measuring station P8, even though the maximum pressure is less than in the case shown in Fig. 7. The average propagation velocity of the detonation wave from P7 to P8 is 1.83 km s^{-1}; this value is well below the C–J detonation velocity.

Figure 11a shows the soot-track record corresponding to Fig. 9, and Fig. 11b is the magnification of the rectangular section of Fig. 11a. This soot-track record shows that no cellular pattern can be observed between each obstacle, so detonation transition failed in the observation section. Shock wave generation is caused by the relatively weak local explosions occurring between the obstacles. In this DDT mecha-
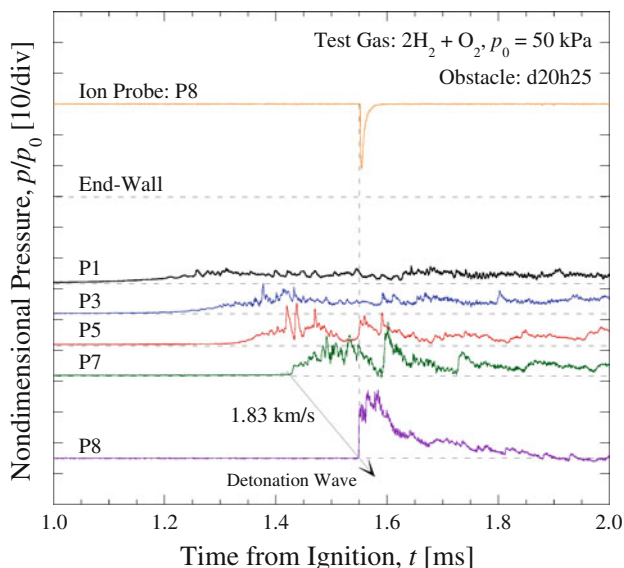

Fig. 11 Soot-track record corresponding to Fig. 9; obstacle: d20h25; test gas: $2H_2 + O_2$

Fig. 10 Pressure histories corresponding to Fig. 9; t elapsed time from ignition; obstacle: d20h25; test gas: $2H_2 + O_2$, $p_0 = 50$ kPa
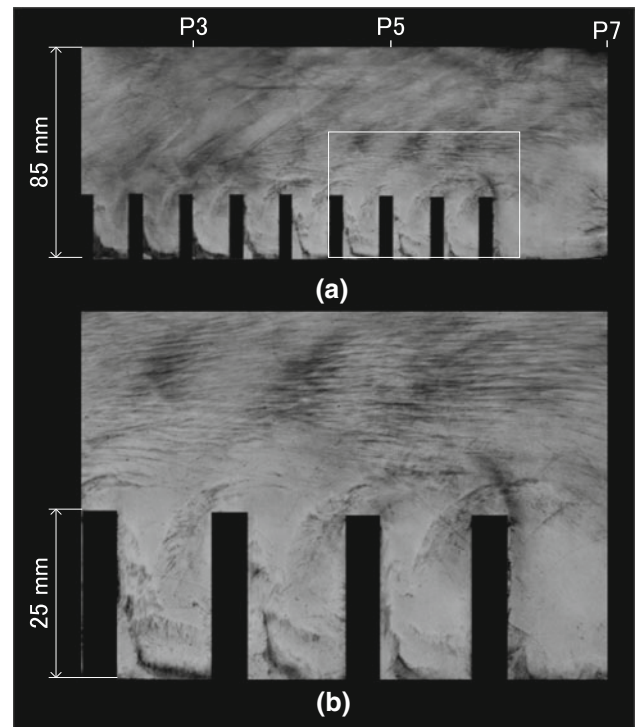
nism, the detonation induction distance from the sparking plug increases until accumulation of the weak shock waves is accomplished, causing an intense local explosion.

The schlieren photographs shown in Fig. 12 are taken in an attempt to visualize DDT onset caused by accumulation of weak shock waves. Thus, the initial pressure of the test gas is increased to $p_0 = 70$ kPa without changing the obstacles from d20h25. The interframe time is reduced to 2 μs with an exposure time of 100 ns. The photographs are entirely dark, despite image processing being performed by adjusting the lightness; the DDT process caused by the accumulation of weak shock waves is barely visible. This behaviour is analogous to that in Fig. 9: a deflagration wave, F, propagates to the right, preceded by multiple weak shock waves, S. As previously discussed, the weak shock waves are generated by local explosions between the obstacles and accumulate, producing more-intense shock waves. In the second frame, $t = 1.191$ ms, another shock wave, of semi-circular shape, is caused by a local explosion near the upper left corner of the photograph. The shock wave propagated with a velocity of approximately 3 km s^{-1} is sequentially overtaking the precursor shock waves, and is eventually accompanied, from the eighth frame, $t = 1.203$ ms, by light emission. These processes are, therefore, considered to indicate this type of DDT onset, i.e. a detonation wave, D, arises naturally near the top wall without causing a strong explosion. Although the central position of the local explosion is near the boundary

Fig. 12 Schlieren photographs showing DDT process occurring by accumulation of weak shock waves; *t* elapsed time from ignition; exposure time: 100 ns; obstacle: d20h25; test gas: $2H_2 + O_2$, $p_0 = 70$ kPa; *D* detonation wave; *F* deflagration wave; *S* shock wave
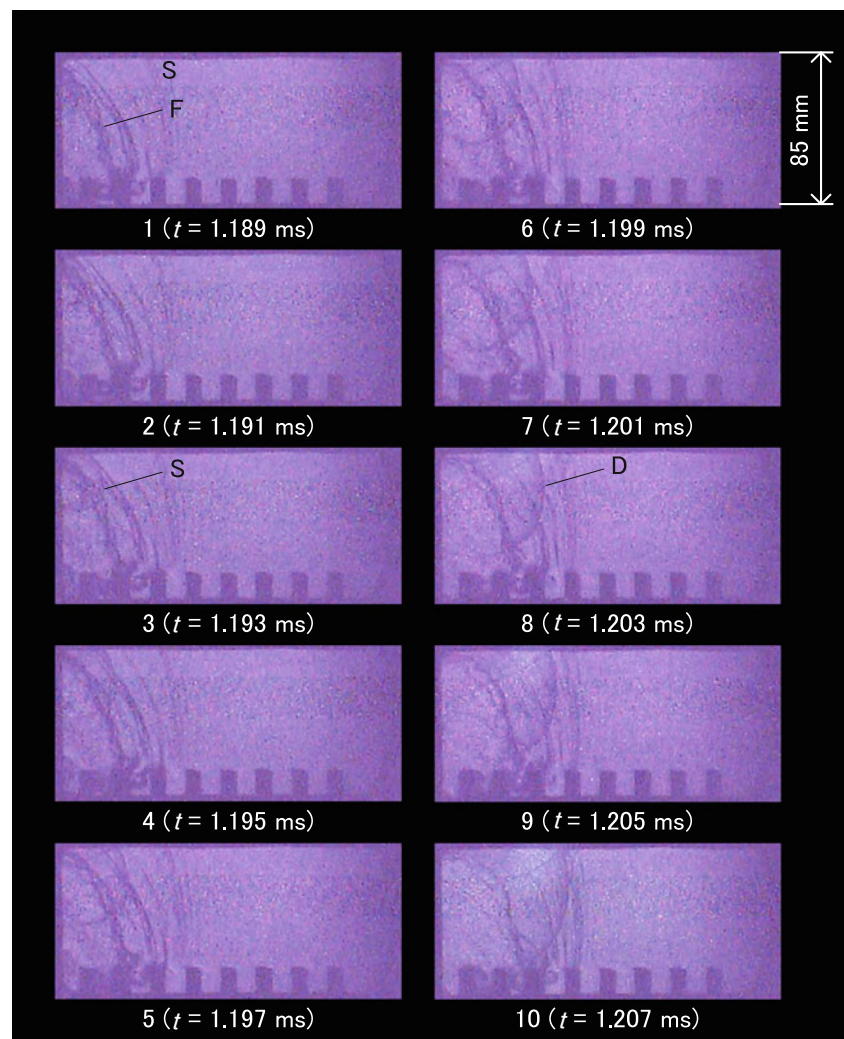
of the observation window, and it is not possible to determine the precise position, it is certainly not on the top wall, but is near the deflagration front. It seems likely, therefore, that the local explosion is triggered by possible processes such as shock waves caused by the weak local explosions between the obstacles overtaking the deflagration front, or, more practically, the reflected shock waves from the top wall interacting with a turbulent reaction zone of the deflagration front; the processes are shown in Fig. 9.

4 Discussion

The detonation induction distance (DID) is of considerable importance, because a pulsed detonation engine requires DDT to occur a short distance from an ignition source in an effort to increase the thermal efficiency. Furthermore, an evaluating of DID, which could be varied by both physical and chemical conditions, has proved useful in considering detonation hazards. This section deals with the relationship
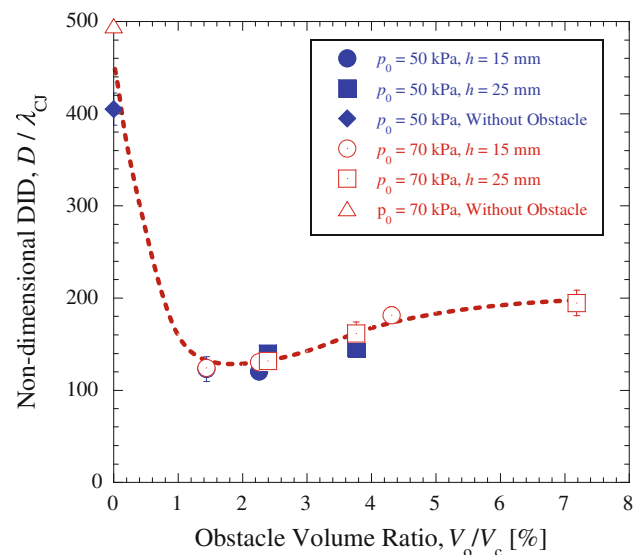

Fig. 13 Relationship between non-dimensional DID, D/λ_{CJ}, and occupation volume ratio of the obstacles in a combustion tube, V_o/V_c; test gas: $2H_2 + O_2$

between DID and experimental conditions such as the physical parameters of the repeated obstacles and the chemical parameters of the test gas.

Figure 13 shows the relationship between DID from a sparking plug, D, and the occupation volume of the repeated obstacles, V_o. In evaluating DID, the distance between the sparking plug and the original position of the cellular pattern is measured on a soot-track record. The vertical axis indicates the non-dimensional DID, D/λ_{CJ}, where the denominator λ_{CJ} is the cell-width of the C–J detonation wave. The cell-width of the C–J detonation wave λ_{CJ} is inversely proportional to the power of the chemical reaction rate, i.e. a smaller cell-width is formed in a premixed gas of higher reaction rate. Therefore, the cell-width of the C–J detonation wave is used as a physically unique parameter to designate the chemical reaction rate of the premixed gas. The horizontal axis indicates the non-dimensional volume ratio of the repeated obstacles, V_o/V_c, where V_c is the total volume of the tube in which the repeated obstacles are inserted. The volume ratio corresponding to $V_o = 0$ denotes that no obstacle is inserted in the combustion tube.

The non-dimensional DID is completely dependent on the presence or absence of the repeated obstacles. In the absence of obstacles, the resulting DID exceeds the C–J detonation cell-width by a factor of approximately 400, and the value decreases to less than one-half in the presence of obstacles. As this figure clearly demonstrates, the resulting DID can be represented as a unique curve by normalizing the DID with the C–J detonation cell-width, λ_{CJ}. Furthermore, the non-dimensional DID tends to decrease as the volume ratio decreases, and takes a local minimum value at $V_o/V_c \simeq 0.02$. The DID value is considerably greater in the absence of obstacles, as is shown in Fig. 4 ($V_o/V_c = 0$). In contrast, in the case of a greater volume ratio, as shown in Fig. 9 ($V_o/V_c = 7.2\%$), DDT does not occur between the obstacles, and is delayed until the accumulation of weak shock waves becomes sufficient to trigger a local explosion. Thus, the resulting DID must take the minimum value for an appropriate volume ratio of the obstacles, which might cause the relatively strong local explosion between the obstacles. This figure demonstrates that the appropriate volume ratio of the obstacles is obtained in the case $V_o/V_c \simeq 0.02$, and the local minimum value exceeds the C–J detonation cell-width by a factor of approximately 120, i.e., $D_{min} \simeq 120\,\lambda_{CJ}$. In addition, the non-dimensional DID yields smaller values as the volume ratio increases. This is because the effects of the obstacles on DDT behaviour become negligible for large volume ratios, and becomes equivalent to the test gas being ignited in a smooth small-diameter tube.

Figure 14 shows the relationship between DID and obstacle pitch, d. The vertical axis is the same as in Fig. 13, D/λ_{CJ}, and the horizontal axis indicates the non-dimensional pitch of the obstacle, d/h, where h is the height of the obstacles
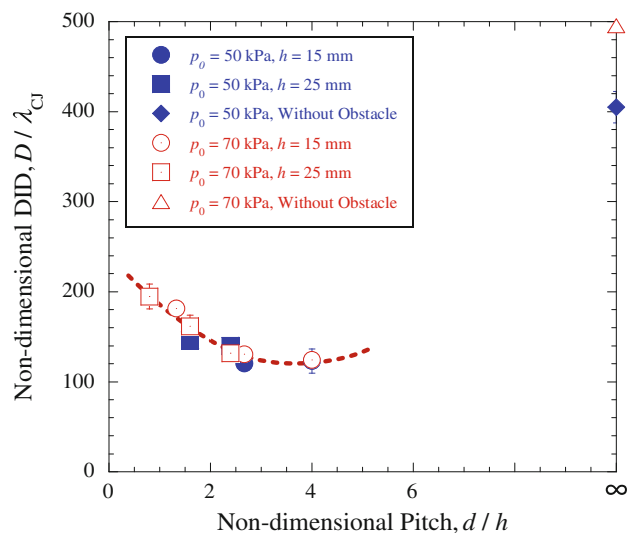

Fig. 14 Relationship between non-dimensional DID, D/λ_{CJ}, and non-dimensional pitch of the obstacle, d/h; test gas: $2H_2 + O_2$

shown in Fig. 3. The plots at $d/h = \infty$ correspond to the case without obstacles. Non-dimensional value of D/λ_{CJ} is also displayed as a unique curve, normalizing the DID with the cell-width of the C–J detonation wave. This figure also demonstrates that the non-dimensional value of D/λ_{CJ} decreases as the value of d/h increases, and it takes the local minimum value at $d/h \simeq 4$. For greater values of non-dimensional pitch, the effects of the obstacles become negligible because the obstacle height is zero or the pitch approaches infinity. For smaller values of non-dimensional pitch, in contrast, obstacles of smaller pitch can only produce small vortices, as shown in Fig. 6, thus the deflagration wave is not accelerated sufficiently to cause local explosions via the mechanism of shock–flame interaction. Therefore, the DID value must take the local minimum value at the appropriate value of the non-dimensional pitch. Inspection of Fig. 14 shows that the optimum obstacle configuration to cause DDT a short distance from the sparking plug is $d/h \simeq 4$.

Although it would be difficult to explain the physical meaning of the optimum pitch of the repeated obstacles that is obtained at greater than the height by a factor of approximately four, each condition is critical in triggerring DDT immediately after ignition, as follows.

1. Vortices which are relatively large scale are produced behind the obstacles, and thus the deflagration wave is sufficiently accelerated by the vortex to transfer the shock wave into the concave region.
2. A reflected shock wave from the obstacle terminates propagation of the deflagration wave; this produces high-temperature unreacted gas pockets in front of the obstacle.

3. The shock waves reflected from both the obstacle front and the bottom wall interact with the deflagration wave to cause an intense local explosion.

Each of these conditions would not be satisfied for either greater or smaller values of the non-dimensional pitch; this would increase the non-dimensional DID.

5 Conclusions

In the present study, an oxy-hydrogen premixed gas was ignited, and the behaviours of the deflagration-to-detonation transition above repeated obstacles were visualized using a high-speed video camera. The pitch and height of obstacles, along with the initial pressure of the test gas, were varied so as to obtain the optimum conditions needed to cause DDT. Based on the results of the experiments, the following conclusions were reached.

1. It became apparent that DDT was essentially caused by one or other of the following mechanisms.

   (a) The repeated obstacles played a major role in generating vortices behind them, and the deflagration wave was accelerated by the vortex. A shock wave was induced on account of the acceleration of the deflagration wave, and thus the shock–flame interactions in front of the obstacle caused DDT via a relatively strong local explosion.
   (b) Each shock wave generated by relatively weak explosions between the obstacles was insufficient to initiate DDT directly, but an accumulation of weak shock waves triggered DDT via a relatively weak local explosion.

2. The detonation induction distance, DID, varied depending on the mechanism; the mechanism was selected by varying either the physical parameters of the obstacle or the chemical parameters of the test gas. In particular, the DID values were relatively small if DDT occurred by the first mechanism.

3. The relationship between the non-dimensional DID and the volume ratio of the obstacle was proved to be represented by a unique curve. In this combustion tube, the minimum value of the non-dimensional DID was obtained for an obstacle volume ratio of approximately 2%.

4. The DID could also be expressed using the physical parameters of the obstacle such as the pitch, d, and the height, h. In this combustion tube, the optimum obstacle configuration to cause DDT a short distance from the ignition source was obtained in the case of $d/h \simeq 4$.

References

1. Urtiew, P.A., Oppenheim, A.K.: Experimental observation of the transition to detonation in an explosive gas. Proc. Roy. Soc. Lond. A **295**, 13–28 (1966)
2. Moen, I.O., Donato, M., Knystautas, R., Lee, J.H.: Flame acceleration due to turbulence produced by obstacles. Combust. Flame **39**, 21–32 (1980)
3. Lee, J.H.S.: The Detonation Phenomenon. Campridge University Press, Cambridge (2008)
4. Kuznetsov, M., Alekseev, V., Matsukov, I., Dorofeev, S.: DDT in a smooth tube filled with a hydrogen–oxygen mixture. Shock Waves **14**, 205–215 (2005)
5. Zhu, Y.J., Chao, J., Lee, J.H.S.: An experimental investigation of the propagation mechanism of critical deflagration waves that lead to the onset of detonation. Proc. Combust. Inst. **31**, 2455–2462 (2007)
6. Teodorczyk, A., Lee, J.H.S., Knystautas, R.: Propagation mechanism of quasi-detonations. In: Proceedings of the Symposium (International) on Combustion, vol. 22, pp. 1723–1731, (1989)
7. Teodorczyk, A., Drobniak, P., Dobkowski, A.: Fast turbulent deflagration and DDT of hydrogen-air mixtures in small obstructed channel. Int. J. Hydrogen Energy **34**, 5887–5893 (2009)
8. Ciccarelli, G., Boccio, J.L.: Detonation wave propagation through a single orifice plate in a circular tube. In: Proceedings of the 27th Symposium (International) on Combustion, Combustion Institute, pp. 2233–2239 (1998)
9. Ciccarelli, G., Flowler, C.J., Bardon, M.: Effect of obstacle size and spacing on the initial stage of flame acceleration in a rough tube. Shock Waves **14**, 161–166 (2005)
10. Johansen, C.T., Ciccarelli, G.: Visualization of the unburned gas flow field ahead of an accelerating flame in an obstructed square channel. Combust. Flame **156**, 405–416 (2009)
11. Ciccarelli, G., Johansen, C.T., Parravani, M.: The role of shock–flame interactions on flame acceleration in an obstacle laden channel. Combust. Flame **157**, 2125–2136 (2010)
12. Card, J., Rival, D., Ciccarelli, G.: DDT in fuel–air mixtures at elevated temperatures and pressures. Shock Waves **14**, 167–173 (2005)
13. Gamezo, V.N., Ogawa, T., Oran, E.S.: Flame acceleration and DDT in channels with obstacles: effect of obstacle spacing. Combust. Flame **155**, 302–315 (2008)
14. Gamezo, V.N., Ogawa, T., Oran, E.S.: Numerical simulations of flame propagation and DDT in obstructed channels filled with hydrogen–air mixture. Proc. Combust. Inst. **31**, 2463–2471 (2007)
15. Dorofeev, S.B., Sidorov, V.P., Kuznetsov, M.S., Matsukov, I.D., Alekseev, V.I.: Effect of scale on the onset of detonations. Shock Waves **10**, 137–149 (2000)
16. Liu, Y.K., Lee, J.H.S., Knystautas, R.: Effect of geometry on the transition of detonation through an orifice. Combust. Flame **56**, 215–225 (1984)
17. Obara, T., Yajima, S., Yoshihashi, T., Ohyagi, S.: A high-speed photographic study of the transition from deflagration to detonation wave. Shock Waves **6**, 205–210 (1996)
18. Grondin, J.S., Lee, J.H.S.: Experimental observation of the onset of deonation downstream of a perforated plate. Shock Waves **20**, 381–386 (2010)

19. Kuznetsov, M.S., Alekseev, V.I., Dorofeev, S.B.: Comparison of critical conditions for DDT in regular and irregular cellular detonation system. Shock Waves **10**, 217–223 (2000)

20. Sorin, R., Zitoun, R., Desbordes, D.: Optimization of the deflagration to detonation transition: reduction of length and time of transition. Shock Waves **15**, 137–145 (2006)

21. Nagai, K., Okabe, T., Kim, K., Yoshihashi, T., Obara, T., Ohyagi, S.: A study on DDT processes in a narrow channel. In: Proceedings of the 26th International Symposium on Shock Waves, CD-ROM (2007)

22. Peraldi, O., Knystautas, R., Lee, J.H.: Criteria for transition to detonation in tubes. In: Proceedings of the 21st Symposium (International) on Combustion, Combustion Institute, pp. 1629–1637 (1986)

23. Gamezo, V.N., Khokhlov, A.M., Oran, E.S.: The influence of shock bifurcations on shock-flame interactions and DDT. Combust. Flame **126**, 1810–1826 (2001)

24. Ohyagi, S., Obara, T., Hoshi, S., Cai, P., Yoshihashi, T.: Diffraction and re-initiation of detonations behind a backward-facing step. Shock Waves **12**, 221–226 (2002)

25. Sentanuhady, J., Tsukada, Y., Yoshihashi, T., Obara, T., Ohyagi, S.: Re-initiation of detonation waves behind a perforated plate. In: Proceedings of the 20th International Colloquium on the Dynamics of Explosions and Reactive Systems, CD-ROM (2005)

26. Obara, T., Sentanuhady, J., Tsukada, Y., Ohyagi, S.: Re-initiation process of detonation wave behind slit-plate. Shock Waves **18**, 117–127 (2008)